Resonant Analysis of Magnetic Coupling Wireless Power Transfer Systems

Zhi-Juan Liao, Yue Sun, *Member, IEEE*, Zhao-Hong Ye, Chun-Sen Tang, *Member, IEEE*, and Pei-Yue Wang

***Abstract*—For a general multi-coil magnetic coupling wireless power transfer (MC-WPT) system with different coil properties and non-negligible cross couplings, there is no analytical solution that connects the resonant frequencies of the system to its electric parameters. Establishing such a generalized analytical solution not only permits quantitative analysis of resonant points but also provides a generic platform for the physical interpretation of resonance. For this purpose, a novel modeling and analysis method of integrating time domain and frequency domain is proposed in this paper, with that all possible resonant points of arbitrary coil MC-WPT systems can be quickly and accurately determined. First, an accurate state-space model of a general MC-WPT system with arbitrary number of transmitters, repeaters, and receivers is established and the analytical current response on each circuit is derived. Then, several key system concepts about resonance are elucidated, based on which the generalized analytical expressions of resonant points of MC-WPT systems, including resonant frequencies and corresponding powers and efficiencies, are derived. Furthermore, the physical interpretation along with the mathematic relationships of several key easy-confusing concepts are deduced, which provides a systematic theoretical criteria for the selection of operating frequency to achieve the resonant states for MC-WPT systems.**

***Index Terms*—Frequency splitting, magnetic coupling (MC), resonance, resonant frequency, wireless power transfer (WPT).**

I. Introduction

MAGNETIC coupling wireless power transfer (MC-WPT) technology has been a research hotspot since the inspiring work of transmitting 60 W power to a lamp with about 40% efficiency was demonstrated in 2007 [1], [2]. Considerable process of this technology has paved the way toward practical applications, such as household appliances [3], [4], medical implanted devices [5], [6], electric vehicles [7], [8], etc. However, it remains a fundamental challenge that is to determine

Manuscript received March 31, 2018; revised August 1, 2018; accepted August 30, 2018. Date of publication September 3, 2018; date of current version April 20, 2019. This work was supported in part by the Grant from the National High Technology Research and Development Program of China (863 Program): 2015AA016201, and in part by the National Natural Science Foundation of China under Grant 61573074. Recommended for publication by Associate Editor S. K. Panda. *(Corresponding author: Yue Sun.)*

Z.-J. Liao, Z.-H. Ye, C.-S. Tang, and P.-Y. Wang are with the College of Automation, Chongqing University, Chongqing 400044, China (e-mail:

Powerful simulation tools can be used to determine the maximum power or efficiency points for a given MC-WPT systems, but they cannot reveal the physical interpretation of resonance of MC-WPT systems. It is well known that the frequencies of the maximum output power and efficiency of an MC-WPT system are not equal. There is no conclusion that which frequency is the resonant frequency of MC-WPT systems. So far, there is still not an explicit concept on resonance and resonant frequency of MC-WPT systems. More importantly, power simulation tools cannot get the analytical relationship between the resonant points and electrical parameters. There are multiple resonant points of an MC-WPT system and the number and positions will vary with the system parameters [19]. So far, the generalized characteristic of the resonant points has not been declared. A generalized analytical relationship is not only the key for maintaining a reasonable level of energy efficiency but also the basis for guiding the system optimization and design.

Coupled mode theory [20], [21] and circuit theory [22], [23] are the two traditional and major analysis methods for MC-WPT systems. However, the two methods can only derive the analytical maximum power or efficiency points by seeking the extreme points of corresponding transfer functions mathematically [21], [23], [24]. The process is very complex and rigorous and then the two methods can only be applied to some specific simple systems. For a complicated multi-coil system with different coils properties and non-negligible cross couplings, the analytical transfer functions are very difficult to derive with the two traditional analysis methods [25]–[28], let along the extreme points of the transfer functions versus the operating frequency.

Recently, we have proposed a theoretical analysis method in terms of time domain to determine the maximum power transfer points for MC-WPT systems, but the theoretical model and analysis results only suits for weak damping systems [29]. For strong damping systems, such as multi-receiver MC-WPT systems, the analysis method and the analysis results proposed in paper [29] are no longer applicable. Moreover, there is no content about resonance of MC-WPT systems in paper [29].

In this paper, a novel modeling and analysis method of integrating time domain and frequency domain is proposed, which could quickly and accurately determine the resonant points for arbitrary coil MC-WPT systems without any parameter constraints. The proposed method is based on the most common equivalent circuit model, which is very well suited for the expected frequency range of MC-WPT systems [30]. With the proposed method, the general analytical expressions of resonant points, including resonant frequencies and corresponding powers and efficiencies at resonant states, are established. In addition, the physical interpretation along with the mathematic relationships of several easy-confusing key concepts, including circuit's natural frequency (CNF), system's natural frequency (SNF), and resonant frequency, is elucidated. The analysis results provide a systematic theoretical criterion for the selection of operating frequency for MC-WPT systems to achieve systems' resonant state.

This paper is organized as follows: In Section II, an accurate state-space model of a general wireless power transfer gird (WPTG) with arbitrary number of transmitters, repeaters, and receivers is established and the analytical current response on each circuit is derived by using matrix calculation. In Section III, several key system concepts about resonance of MC-WPT systems are elucidated, based on which the analytical expressions of resonant points, including resonant frequencies and corresponding power and efficiency at resonant points are derived. Furthermore, the physical interpretation along with the mathematical relationship of several easy-confusing concepts, including CNF, SNF, and resonant frequency are deduced. In Section IV, the related parameters affecting the resonant frequencies are explored to pursue investigation into their impact on the resonant points. Finally, prototypes and corresponding Simulink simulations are built and tested to validate the proposed theoretical model and analysis results.

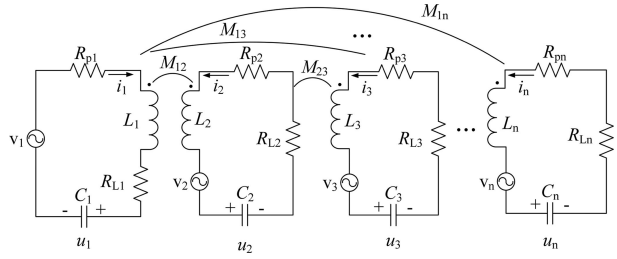

Fig. 1. Equivalent circuit diagram of a general n-coil fully coupled WPTG system.

II. System Modeling and Response Analysis

A. General State-Space Model of WPTG Systems

Fig. 1 shows the equivalent circuit diagram of a general n-coil fully coupled WPTG system. The system consists of n coils and each coil is connected with a capacitor in series to form an oscillating circuit.

In Fig. 1, variables with the subscript m represents the parameters in the mth oscillating circuit ($m = 1, 2, \ldots, n$). Rp_m and L_m indicate the equivalent series resistance (ESR) and self inductance of the mth coil, respectively, M_{mr} is defined as the mutual inductance between the mth coil and rth coil ($m \neq r$ and $M_{\mathrm{mr}} = M_{\mathrm{rm}}$). C_m and R_{Lm} are the compensating capacitance and load resistance of the mth circuit, respectively. U_m and v_m stand for the voltage of the capacitor C_m and the supply voltage of the mth circuit, i_m presents the current in the mth circuit. It should be noted that v_m and R_{Lm} cannot exist at the same time. When $v_m \neq 0$ and $R_{Lm} = 0$, the mth circuit is regarded as a transmitter. Conversely, when $v_m = 0$ and $R_{Lm} \neq 0$, the mth circuit serves as a receiver. When both of them are equal to zero, the mth circuit is a repeater.

According to Kirchhoff's voltage law, the mathematic equation of the WPTG system described in Fig. 1 can be expressed as follows:

$$\begin{cases} L_1C_1\ddot{u}_1 + M_{12}C_2\ddot{u}_2 + \cdots M_{1n}C_n\ddot{u}_n + R_1C_1\dot{u}_1 + u_1 = v_1 \\ M_{12}C_1\ddot{u}_1 + L_2C_2\ddot{u}_2 + \cdots M_{2n}C_n\ddot{u}_n + R_2C_2\dot{u}_2 + u_2 = v_2 \\ \qquad\qquad\qquad\qquad \vdots \\ M_{1n}C_1\ddot{u}_1 + M_{2n}C_2\ddot{u}_2 + \cdots L_nC_n\ddot{u}_n + R_nC_n\dot{u}_n + u_n = v_n \end{cases} \tag{1}$$

where $R_m = R_{\mathrm{pm}} + R_{\mathrm{Lm}}$ is the total resistance of the mth circuit.

Defining $\mathbf{v} = [\, v_1 \; v_2 \; \cdots \; v_3 \,]^T$, $\mathbf{i} = [\, i_1 \; i_2 \; \cdots \; i_n \,]^T$, and $\mathbf{u} = [\, u_1 \; u_2 \; \cdots \; u_n \,]^T$ as the supply voltage vector, current vector, and capacitor voltage vector of the system, respectively, the mathematic model in (1) can be rewritten as $\mathbf{LC\ddot{u}} + \mathbf{RC\dot{u}} + \mathbf{u} = \mathbf{v}$, where matrix $\mathbf{L}$, $\mathbf{C}$, and $\mathbf{R}$ are the inductance matrix, capacitor matrix, and resistance of the system shown as follows:

$$\mathbf{L} = \begin{bmatrix} L_1 & M_{12} & \cdots & M_{1n} \\ M_{21} & L_2 & \cdots & M_{2n} \\ \vdots & \vdots & \ddots & \vdots \\ M_{n1} & M_{n2} & \cdots & L_n \end{bmatrix}$$

$$\mathbf{C} = \begin{bmatrix} C_1 & 0 & \cdots & 0 \\ 0 & C_2 & \cdots & 0 \\ \vdots & \vdots & \ddots & \vdots \\ 0 & 0 & \cdots & C_n \end{bmatrix}, \mathbf{R} = \begin{bmatrix} R_1 & 0 & \cdots & 0 \\ 0 & R_2 & \cdots & 0 \\ \vdots & \vdots & \ddots & \vdots \\ 0 & 0 & \cdots & R_n \end{bmatrix}. \tag{2}$$

Let $\mathbf{x} = [\, \mathbf{u}^T \; \dot{\mathbf{u}}^T \,]^T$ and $\mathbf{v}' = [\, \mathbf{v}^T \; \mathbf{0}_{1\times n} \,]^T$ be the state vector and input vector of the system, respectively. By introducing the identity $\mathbf{LC\dot{u}} - \mathbf{LC\dot{u}} = \mathbf{0}$, the state-space model of the system can be established as

$$\mathbf{A\dot{x}} + \mathbf{Bx} = \mathbf{v}' \tag{3}$$

where

$$\mathbf{A} = \begin{bmatrix} \mathbf{RC} & \mathbf{LC} \\ \mathbf{LC} & \mathbf{0} \end{bmatrix}, \mathbf{B} = \begin{bmatrix} I_{n\times n} & \mathbf{0} \\ \mathbf{0} & -\mathbf{LC} \end{bmatrix}. \tag{4}$$

From (3), the system matrix $\mathbf{S}$ of the system can be derived as

$$\mathbf{S} = -\mathbf{A}^{-1}\mathbf{B} = \begin{bmatrix} \mathbf{0} & I_{n\times n} \\ -[\mathbf{LC}]^{-1} & -[\mathbf{LC}]^{-1}\mathbf{RC} \end{bmatrix} \tag{5}$$

where $I_{n\times n}$ represents an n-order unit matrix.

B. Derivation of the Analytical Current on Each Circuit

According to the modal theory, there is a non-singular matrix $\mathbf{\Phi} = [\{\psi_1\}\{\psi_2\}\cdots\{\psi_n\}\{\psi_1^*\}\;\{\psi_2^*\}\cdots\{\psi_n^*\}]_{2n\times 2n} = [\varphi_{ij}]_{2n\times 2n}$ of an actual physical system, which makes (6) established [31]

$$\begin{aligned} \mathbf{\Phi}^T\mathbf{A}\mathbf{\Phi} &= \bar{\mathbf{A}} = diag\begin{bmatrix} \mathbf{a} & \mathbf{a}^* \end{bmatrix} \\ &= diag\begin{bmatrix} a_1 & a_2 & \cdots & a_n & a_1^* & a_2^* & \cdots & a_n^* \end{bmatrix} \\ \mathbf{\Phi}^T\mathbf{B}\mathbf{\Phi} &= \bar{\mathbf{B}} = diag\begin{bmatrix} \mathbf{b} & \mathbf{b}^* \end{bmatrix} \\ &= diag\begin{bmatrix} b_1 & b_2 & \cdots & b_n & b_1^* & b_2^* & \cdots & b_n^* \end{bmatrix} \end{aligned} \tag{6}$$

where $\{\psi_q\}$ and $\{\psi_q^*\}$ are conjugate complex, $a_q = \{\psi_q\}^T\mathbf{A}\{\psi_q\}$, $a_q^* = \{\psi_q^*\}^T\mathbf{A}\{\psi_q^*\}$, $b_q = \{\psi_q\}^T\mathbf{B}\{\psi_q\}$, $b_q^* = \{\psi_q^*\}^T\mathbf{B}\{\psi_q^*\}$ $(q = 1, 2, ..., n)$ and the operator $\mathrm{diag}[\cdot]_{2n\times 2n}$ represents the generation of an $2n$-order diagonal matrix with the $2n$ elements in the brackets as the diagonal elements. It should be noted that different from the subscript m in Fig. 1, which denotes the circuit elements in the mth oscillating circuit, the subscript q emphasizes the position of the column $\{\varphi\}_q$ in matrix $\mathbf{\Phi}$.

By transforming (6), we have

$$\left(-\mathbf{A}^{-1}\mathbf{B}\right)\mathbf{\Phi} = \mathbf{S\Phi} = \mathbf{\Phi\Lambda} \tag{7}$$

where

$$\begin{aligned} \mathbf{\Lambda} &= -\left(\bar{\mathbf{A}}\right)^{-1}\bar{\mathbf{B}} = -\left(\mathrm{diag}\begin{bmatrix} \mathbf{a} & \mathbf{a}^* \end{bmatrix}\right)^{-1} * \mathrm{diag}\begin{bmatrix} \mathbf{b} & \mathbf{b}^* \end{bmatrix} \\ &= \mathrm{diag}[\lambda \quad \lambda^*] \\ &= \mathrm{diag}\begin{bmatrix} \lambda_1 & \lambda_2 & \cdots & \lambda_n & \lambda_1^* & \lambda_2^* & \cdots & \lambda_n^* \end{bmatrix}. \end{aligned} \tag{8}$$

Equation (7) represents an eigenvalue problem where $\lambda_1, \lambda_2, \ldots, \lambda_n, \lambda_1^*, \lambda_2^*, \ldots, \lambda_n^*$ and $\{\psi_1\}, \{\psi_2\}, \ldots, \{\psi_n\}$, $\{\psi_1^*\}, \{\psi_2^*\}, \ldots \{\psi_n^*\}$ are the eigenvalues and corresponding eigenvectors of the system matrix $\mathbf{S}$, based on which the matrix $\mathbf{\Phi}$, $\mathbf{\Lambda}$ as well as matrix $\bar{\mathbf{A}}$ and $\bar{\mathbf{B}}$ can be quickly and accurately determined.

By using (6), the state-space model in (3) can be decoupled into $2n$ mutually independent equations, as shown in (9), where $\mathbf{y} = \mathbf{\Phi}^{-1}\mathbf{x}$

$$\bar{\mathbf{A}}\dot{\mathbf{y}} + \bar{\mathbf{B}}\mathbf{y} = \mathbf{\Phi}^T\mathbf{v}'. \tag{9}$$

For mathematic analysis, sinusoidal supply voltages with the frequency ω are assumed. Then, the supply voltage v_m, circuit current i_m, and capacitor voltage u_m on the mth oscillating circuit can be expressed as $v_m = \mathrm{Im}(|v_m|e^{j\theta_{v_m}}e^{j\omega t})$, $i_m = \mathrm{Im}(|i_m|e^{j\theta_{i_m}}e^{j\omega t})$, and $u_m = \mathrm{Im}(|u_m|e^{j\theta_{u_m}}e^{j\omega t})$, where the operator $||$ represents the amplitude of the variable in the bracket and $\mathrm{Im}(\cdot)$ stand for the imaginary part of the variable in the bracket, i.e., $v_m = \mathrm{Im}(|v_m|e^{j\theta_{v_m}}e^{j\omega t}) = |v_m|\sin(\omega t + \theta_{v_m})$.

Defining $\mathbf{V} = [\, V_1 \; V_2 \; \ldots \; V_n \,]^T$, $\mathbf{I} = [\, I_1 \; I_2 \; \ldots \; I_n \,]^T$, and $\mathbf{U} = [\, U_1 \; U_2 \; \ldots \; U_n \,]^T$, where $V_m = |v_m|e^{j\theta_{v_m}}$, $I_m = |i_m|e^{j\theta_{i_m}}$ and $U_m = |u_m|e^{j\theta_{u_m}}$ $(m = 1, 2, \ldots, n)$, the supply voltage vector $\mathbf{v}$, current vector $\mathbf{i}$, and the capacitor voltage vector $\mathbf{u}$ of the system can be expressed as $\mathbf{v} = \mathrm{Im}(\mathbf{V}e^{j\omega t})$, $\mathbf{i} = \mathrm{Im}(\mathbf{I}e^{j\omega t})$, and $\mathbf{u} = \mathrm{Im}(\mathbf{U}e^{j\omega t})$. According to $\mathbf{x} = [\, \mathbf{u}^T \; \dot{\mathbf{u}}^T \,]^T$, $\mathbf{v}' = [\, \mathbf{v}^T \; \mathbf{0}_{1\times n} \,]^T$, and $\mathbf{y} = \mathbf{\Phi}^{-1}\mathbf{x}$, the state vector $\mathbf{y}$ and input vector $\mathbf{v}'$ can be obtained as $\mathbf{y} = \mathrm{Im}(\mathbf{Y}e^{j\omega t})$ and $\mathbf{v}' = \mathrm{Im}(\mathbf{V}'e^{j\omega t})$, where $\mathbf{Y} = \mathbf{\Phi}^{-1}[\, \mathbf{U}^T \; j\omega\mathbf{U}^T \,]^T$ and $\mathbf{V}' = [\, \mathbf{V}^T \; \mathbf{0}_{n\times 1} \,]^T$. Substituting $\mathbf{y} = \mathrm{Im}(\mathbf{Y}e^{j\omega t})$ and $\mathbf{v}' = \mathrm{Im}(\mathbf{V}'e^{j\omega t})$ into (9), yields

$$\frac{d\left(\mathbf{Y}e^{j\omega t}\right)}{dt} = \mathbf{\Lambda Y}e^{j\omega t} + \left(\mathrm{diag}\begin{bmatrix} \mathbf{a} & \mathbf{a}^* \end{bmatrix}\right)^{-1}\mathbf{\Phi}^T\mathbf{V}'e^{j\omega t}. \tag{10}$$

From $\mathbf{Y} = \mathbf{\Phi}^{-1}[\, \mathbf{U}^T \; j\omega\mathbf{U}^T \,]^T$ and (10), we have

$$\begin{bmatrix} \mathbf{U} \\ j\omega\mathbf{U} \end{bmatrix} = \mathbf{\Phi}(j\omega I_{2n\times 2n} - \mathbf{\Lambda})^{-1}\left(\mathrm{diag}\begin{bmatrix} \mathbf{a} & \mathbf{a}^* \end{bmatrix}\right)^{-1}\mathbf{\Phi}^T\mathbf{V}'. \tag{11}$$

Matrix $\mathbf{\Phi}_{2n\times 2n}$ can be rewritten as a block matrix $\mathbf{\Phi} = \begin{bmatrix} \mathbf{\Phi}_I & \mathbf{\Phi}_I^* \\ \mathbf{\Phi}_U & \mathbf{\Phi}_U^* \end{bmatrix}$, where $\mathbf{\Phi}_I = [\varphi_{ij}]_{n\times n} = [\{\varphi_\mathbf{1}\}, \{\varphi_\mathbf{2}\} \ldots \{\varphi_\mathbf{n}\}]$, $\{\varphi_\mathbf{q}\} = [\, \varphi_{1q} \; \varphi_{2q} \; \ldots \; \varphi_{nq} \,]^\mathrm{T}$ and $\mathbf{q} = 1, 2, \ldots, n$. Evaluating (11) in terms of block matrix $\mathbf{\Phi}$, the vector $\mathbf{U}$ can be

obtained as

$$\begin{aligned}\mathbf{U} &= \mathbf{\Phi}_i(j\omega I_{n\times n}-\lambda)^{-1}\mathbf{a}^{-1}(\mathbf{\Phi}_i)^T\mathbf{V}+\mathbf{\Phi}_i^*(j\omega I_{n\times n}-\lambda^*)^{-1}\\ &\quad\times(\mathbf{a}^*)^{-1}(\mathbf{\Phi}_i^*)^T\mathbf{V}\\ &= \sum_{q=1}^{n}\left(\frac{\{\varphi_\mathbf{q}\}\{\varphi_\mathbf{q}\}^T\mathbf{V}}{a_q(j\omega-\lambda_q)}+\frac{\{\varphi_\mathbf{q}^*\}\{\varphi_\mathbf{q}^*\}^T\mathbf{V}}{a_q^*(j\omega-\lambda_q^*)}\right).\end{aligned}\tag{12}$$

According to the relationship of capacitor current and capacitor voltage, we have $\mathbf{I}=j\omega\mathbf{C}\mathbf{U}$. Then, the analytical current vector $\mathbf{i}$ of the system can be obtained as

$$\mathbf{i}=\mathrm{Im}\left(\mathbf{I}e^{j\omega t}\right)=\mathrm{Im}\left(\omega\mathbf{C}\mathbf{U}e^{j(\omega t+\pi/2)}\right).\tag{13}$$

From (13), the analytical current response on each circuit in the system can be quickly derived. For example, the current response on the mth oscillating circuit can be derived as $i_m=\mathrm{Im}(I_m e^{j(\omega t+\pi/2)})$, where

$$I_m=\omega C_m\sum_{q=1}^{n}\left(\frac{\varphi_{mq}\{\varphi_\mathbf{q}\}^T\mathbf{V}}{a_q(j\omega-\lambda_q)}+\frac{\varphi_{mq}^*\{\varphi_\mathbf{q}^*\}^T\mathbf{V}}{a_q^*(j\omega-\lambda_q^*)}\right).\tag{14}$$

C. Power and Efficiency of WPTG Systems

The received power by the electrical load on the mth oscillating circuit P_m is calculated by $P_m=|i_m|^2R_{Lm}/2$, where $|i_m|$ presents the amplitude of current i_m. From $i_m=\mathrm{Im}(I_m e^{j(\omega t+\pi/2)})$, we can get that the amplitude of current i_m equals to the modulus of plural I_m, that is $|i_m|=|I_m|$. Then, the received power by the load on the mth oscillating circuit can be expressed as

$$P_m=\frac{1}{2}|I_m|^2R_{Lm}.\tag{15}$$

From (15), the transfer efficiency of the whole WPTG system can be derived as

$$\eta=\frac{\sum_{k=1}^{n}\left(|I_k|^2R_{Lk}\right)}{\sum_{m=1}^{n}\left(|I_m|^2(R_{pm}+R_{Lm})\right)}\tag{16}$$

where $|I_k|$ and R_{Lk} are the current amplitude and load resistance of the kth circuit.

III. Resonant Analysis of MC-WPT Systems

A. Several Key Concepts About Resonance of MC-WPT Systems

Before resonant analysis, several key concepts about resonance of MC-WPT systems need to be elucidated.

1) *Resonance and resonant frequency:* The mathematic model of $\mathbf{L}\mathbf{C}\ddot{\mathbf{u}}+\mathbf{R}\mathbf{C}\dot{\mathbf{u}}+\mathbf{u}=\mathbf{v}$ indicates that the MC-WPT system in fact is a typical vibration system [31]. According to the definition in vibration theory, resonance refers to a sharp increase of energy of a system when the operating frequency equals to some specific frequencies and these specific frequencies are defined as the resonant frequencies of this system [31]. For an MC-WPT system, the energy of the system is determined by the current amplitude on each circuit and corresponding self inductance, for example, the energy of the system, as shown in Fig. 1, can be calculated by $W=\sum_{m=1}^{n}|i_m|^2L_m$. Since the self inductance in each circuit is dependent on its coil, then the resonance of MC-WPT systems refers to the sharp increase of current amplitudes of the system. Correspondingly, the operating frequencies for the maximum current amplitudes are defined as the resonant frequencies of the MC-WPT system.
2) *Natural frequency (RF):* The undamped free oscillating frequency of an oscillating system is defined as the natural frequency of this system. Since an MC-WPT system is composed of multiple mutually coupled *RLC* oscillating circuits, for distinction, the undamped free oscillating frequency of the whole MC-WPT system is termed as SNF, and the undamped free oscillating frequency of a single *RLC* oscillating circuit in the system without considering the effects of other circuits is called CNF.

B. Predicating the Resonant Points of MC-WPT Systems

Since λ_q is the eigenvalue of the system matrix $\mathbf{S}$ of the system, according to the physical properties of a practical system, the real part of λ_q is a negative number with a small absolute value. Then, λ_q and λ_q^* can be expressed as $\lambda_q=-\alpha_q+j\omega_{r,q}$ and $\lambda_q^*=-\alpha_q-j\omega_{r,q}$, respectively, where α_q and $\omega_{r,q}$ are positive number and α_q is usually very small. In this case, the plural I_m in (14) can be rewritten as

$$I_m=\sum_{q=1}^{n}\left(\varphi_{mq}A_q+\varphi_{mq}^*B_q\right)\tag{17}$$

where

$$\begin{aligned}A_q&=\frac{\{\varphi_\mathbf{q}\}^T\mathbf{V}}{a_q\left(\alpha_q+j\left(\omega-\omega_{r,q}\right)\right)}\\ B_q&=\frac{\{\varphi_\mathbf{q}^*\}^T\mathbf{V}}{a_q^*\left(\alpha_q+j\left(\omega+\omega_{r,q}\right)\right)}.\end{aligned}\tag{18}$$

The modulus of plural $|A_q|$ reaches the maximum value $|A_q|_{\max}$ when the operating frequency ω equals to $\omega_{r,q}$, i.e.,

$$|A_q|_{\max}=|A_q|_{\omega=\omega_{r,q}}=\left|\{\varphi_q\}^TV\right|/\left(|a_q|\,|\alpha_q|\right).\tag{19}$$

Since α_q is generally very small, then $|A_q|_{\max}$ is always very large. According to the definition elucidated in Section III-A that the frequencies of the maximum current amplitudes are termed as the resonant frequencies of that system, we can get the following.

1) If $\omega_{r,1},\omega_{r,2},\ldots,\omega_{r,n}$ are far away from each other, when the operating frequency ω equals to $\omega_{r,q}$, $|A_q|_{\omega=\omega_{r,q}}=|A_q|_{\max}$ will be much larger than other items $|A_r|_{\omega=\omega_{r,q}}$ ($r=1,2,\ldots,n$ and $r\neq q$) and all items $|B_k|_{\omega=\omega_{r,q}}$ ($k=1,2,\ldots,n$). In this case, I_m can be approximated as $I_m|_{\omega=\omega_{r,q}}\approx\varphi_{mq}A_{q,\omega=\omega_{r,q}}$, which indicates that the

current amplitude reaches a local maximum value and the system is in a resonant state.

2) Conversely, if $\omega_{r,q}$ and $\omega_{r,p}$ are very close, when the operating frequency ω equals to $\omega_{r,q}$, the amplitudes $|A_q|_{\omega=\omega_{r,q}}$ and $|A_p|_{\omega=\omega_{r,q}}$ both will be very large. In this case, I_m can be approximated as $I_m|_{\omega=\omega_{r,q}} \approx \varphi_{mq}A_{q,\omega=\omega_{r,q}} + \varphi_{mp}A_{p,\omega=\omega_{r,q}}$ and the frequency of the maximum current amplitude $|I_m|$ will be in the range of $[\omega_{r,q},\omega_{r,p}]$. Since $\omega_{r,q}$ and $\omega_{r,p}$ are very close and both of them will be more closer to the frequency of the maximum current amplitude which in the range of $[\omega_{r,q},\omega_{r,p}]$, hence $\omega_{r,q}$ and $\omega_{r,p}$ also can be regarded as the resonant frequencies of the system.

The analysis results indicate that there are n resonant frequencies $(\omega_{r,1},\omega_{r,2},\ldots,\omega_{r,n})$ of a *n-coil* system, which are the imaginary part of the eigenvalue of the system matrix $\mathbf{S}$, shown as follows:

$$\omega_{r,1},\omega_{r,2},\ldots,\omega_{r,n} = \left|\mathrm{Im}\left(\mathrm{eigenvalue}\left(\mathbf{S}\right)\right)\right|. \tag{20}$$

Substituting $\omega = \omega_{r,1},\omega_{r,2},\ldots,\omega_{r,n}$ to (14) into (15) and (16), the powers and efficiencies of the resonant points can be quickly and accurately determined.

C. Physical Interpretation of Resonance

At present, there are many misunderstandings about the resonance of MC-WPT systems, as described in the introduction, which is mainly caused by several easy-confusing system parameters, including CNF, SNF, and resonant frequency. Hence, it is necessary to elucidate the physical interpretation of these concepts along with the relationships among them.

Circuit's natural frequency: According to the definition elucidated in Section III-A, CNF refers to the undamped free oscillating frequency of a single *RLC* oscillating circuit without considering the effect of other oscillating circuits. The undamped free oscillating equation of the single mth oscillating circuit in Fig. 1 can be expressed as $L_mC_m\ddot{u}_m + u_m = 0$, whose free oscillating frequency can be derived as $\omega_{c,m} = 1/\sqrt{L_mC_m}$. The result indicates that there is a unique natural frequency of the single *m*th *RLC* oscillating circuit in the system, which is well known as $1/\sqrt{L_mC_m}$. Since the *n*-coil WPTG system consists of *n RLC* oscillating circuits, then there are *n* circuits' natural frequencies $(\omega_{c,1},\omega_{c,2},\ldots\omega_{c,n})$ in the system, as shown in (21), which have one-to-one relationship with the *n RLC* oscillating circuits in the system

$$\omega_{c,m} = 1/\sqrt{L_mC_m}(m = 1,2,\ldots,n). \tag{21}$$

System's natural frequency: SNF refers to the undamped free oscillating frequency of the whole MC-WPT system. For the WPTG system described in (1), the undamped free oscillating equation can be rewritten as $\mathbf{LC\ddot{u}} + \mathbf{u} = \mathbf{0}$. Supposed that the undamped free oscillating response of capacitor voltage vector is $\mathbf{u}_0 = \mathrm{Im}(U_0e^{j\omega_0 t})$, where ω_0 is the undamped free oscillating frequency of the system. Substituting $\mathbf{u}_0$ into $\mathbf{LC\ddot{u}} + \mathbf{u} = \mathbf{0}$, we have $|\omega_0^2\mathbf{I} - (\mathbf{LC})^{-1}| = 0$, which indicates that ω_0^2 is the eigenvalue of matrix $(\mathbf{LC})^{-1}$. Then, we can get that there are *n* natural frequencies of an *n-coil* WPTG system, which are the square roots of the eigenvalue of the matrix $(\mathbf{LC})^{-1}$, i.e.,

$$\omega_{0,1},\omega_{0,2},\cdots\omega_{0,n} = \sqrt{\mathrm{eigenvalue}\left((\mathbf{LC})^{-1}\right)}. \tag{22}$$

Actually, the *n* system's natural frequencies are the *n* modal frequencies derived in paper [29]. Expanding (22), we have

$$\omega_{0,1},\omega_{0,2},\cdots\omega_{0,n} = \sqrt{\mathrm{eigenvalue}\left(\begin{bmatrix} L_1C_1 & M_{12}C_2 & \cdots & M_{1n}C_n \\ M_{12}C_1 & L_2C_2 & \cdots & M_{2n}C_n \\ \vdots & \vdots & \ddots & \vdots \\ M_{1n}C_1 & M_{2n}C_2 & \cdots & L_nC_n \end{bmatrix}^{-1}\right)}. \tag{23}$$

By comparing (21) and (23), we can get that even if all circuits' natural frequencies are set to be equal, only when all mutual inductances are close to zero, are the system's natural frequencies equal to the designed CNF.

Resonant frequencies: From Section III-B, we can get that $\lambda_q = -\alpha_q + j\omega_{r,q}$ $(q = 1,2,\ldots,n)$ are the eigenvalue of system matrix $\mathbf{S}$. According to the definition of eigenvalue, we have

$$\left|\left(-\alpha_q + j\omega_{r,q}\right)I_{2n\times 2n} - \mathbf{S}\right| = 0. \tag{24}$$

For any state vector $\mathbf{x}$, from (24), we can get $(-\alpha_q + j\omega_{r,q})\mathbf{x} = \mathbf{S}\mathbf{x}$. The result indicates that resonant frequencies $\omega_{r,q}$ $(q = 1,2,\ldots,n)$ in fact are the damped free oscillating frequency of the system. Expanding (24), we have

$$\left|\lambda_q I_{2n\times 2n} - \begin{vmatrix} \mathbf{0} & \mathbf{I} \\ -[\mathbf{LC}]^{-1} & -[\mathbf{LC}]^{-1}\mathbf{RC} \end{vmatrix}\right| = 0. \tag{25}$$

Evaluating (25) in terms of block matrices, we can get

$$\left|-\lambda_q^2 I_{n\times n} - \lambda_q(\mathbf{LC})^{-1}\mathbf{RC} - (\mathbf{LC})^{-1}\right| = 0. \tag{26}$$

Since matrix $\mathbf{LC}$ is a real symmetric matrix, when the system is a weak damping system (resistance matrix $\boldsymbol{R}$ close to zero matrix), λ_q will be a pure imaginary number and can be expressed as $\lambda_q = j\omega_{r,q}$. In this case, we can get

$$\left|\omega_{r,q}^2 I_{n\times n} - (\mathbf{LC})^{-1}\right| = 0. \tag{27}$$

The results in (27) and (22) indicate that, when the system is a weak-damping system (resistance matrix $\boldsymbol{R}$ close to zero matrix), the n resonant frequencies are equal to the n system's natural frequencies. From the above analysis, we can get the following.

1) There are *n* resonant frequencies of an *n*-coil MC-WPT system, as shown in (20), which are the damped free oscillating frequencies of the system and determined by all self inductances, capacitors, mutual inductances, and resistances of the system.
2) There are *n* system's natural frequencies of an *n*-coil MC-WPT system, as shown in (22), which are the undamped free oscillating frequencies of the system. Only when the system is a weak damping system, are the *n* resonant frequencies of the system equal to the *n* system's

TABLE I
ELECTRIC PARAMETERS OF THE EXAMPLES

Parameters	Value	Parameters	Value
L_1, L_2, L_3, L_4 (μH)	57	v_1 (V)	7
$R_{p1}, R_{p2}, R_{p3}, R_{p4}$ (Ω)	0.13	v_2, v_3, v_4 (V)	0
M_{12}, M_{23}, M_{34} (μH)	18.39	R_{L1}, R_{L2}, R_{L3} (Ω)	0
M_{13}, M_{24} (μH)	6.92	R_{L4} (Ω)	5
M_{14} (μH)	3.11		

natural frequencies of the system. That is, the system's natural frequencies can be regarded as the resonant frequencies in the system design when the system is a weak-damping system.

3) There are n circuits' natural frequencies in an n-coil MC-WPT system, as shown in (21), which indicates the undamped free oscillating frequency of a single *RLC* oscillating circuit without considering the effect of other circuits. Even if the n circuits' natural frequencies are set to equal, as designed in the conventional system, only when all the mutual inductances are close to zero, is the designed CNF equal to the SNF, but it is not equal to the resonant frequency. In other words, there is no direct relationship between CNF and resonant frequency, and the traditional understanding of the "resonant coupling principle" is not exactly true.
4) CNF, SNF, and resonant frequency are three different concepts, where the resonant frequencies should be adopted as the operating frequency to realize system's resonant state. The resonant frequency calculation formula of (20) is valid for arbitrary MC-WPT systems without any parameter constraints.

IV. RELATED PARAMETERS CHARACTERISTIC ANALYSIS

From the above analysis we can get that, there are n possible resonant frequencies of an n-coil MC-WPT system, as shown in (20), which are determined by all circuits' natural frequencies, mutual inductances, and resistances of the system. In this section, the related parameters affecting the resonant frequencies will be explored to pursue investigation into their impact on the resonant points.

A. Effects of CNF

In the conventional MC-WPT systems, all circuits' natural frequencies are set to be equal for satisfying the "resonant coupling principle." However, according to the above analysis, we can get that resonant frequencies of an MC-WPT system have no direct relationship with circuit's natural frequencies in the system. For illustration and verification, a four-coil MC-WPT system with the electric parameters listed in Table I is taken in this section. In the first example, all circuits' natural frequencies are set to $f_{c,1} = f_{c,2} = f_{c,3} = f_{c,4} = 85$ kHz by setting $C_1 = C_2 = C_3 = C_4 = 61.5$ nF. In the second example, the natural frequency of the first and second circuits are set to $f_{c,1} = f_{c,2} = 85$ kHz by setting $C_1 = C_2 = 61.5$ nF, whereas the natural frequency of the third and fourth circuits are set to $f_{c,3} = f_{c,4} = 75$ kHz by setting $C_3 = C_4 = 79$ nF. For these given electric parameters, the theoretical resonant frequencies and corresponding powers and efficiencies of the systems are listed in Table II. The output power and transfer efficiency versus the operating frequency of the two examples are plotted in Fig. 2 for comparison.

TABLE II
THEORETICAL RESONANT FREQUENCIES AND CORRESPONDING POWERS AND EFFICIENCIES

System type	Resonant frequencies (kHz)	Output Power P_4 (W)	Transfer efficiency (%)
The system with equal CNF	66.29	6.68	85.26
	83.21	9.352	92.45
	98.45	8.492	91.29
	112.14	8.155	77.32
The system with unequal CNF	61.49	2.773	90.14
	78.91	9.106	92.48
	91.12	9.824	90.87
	108.27	20.67	44

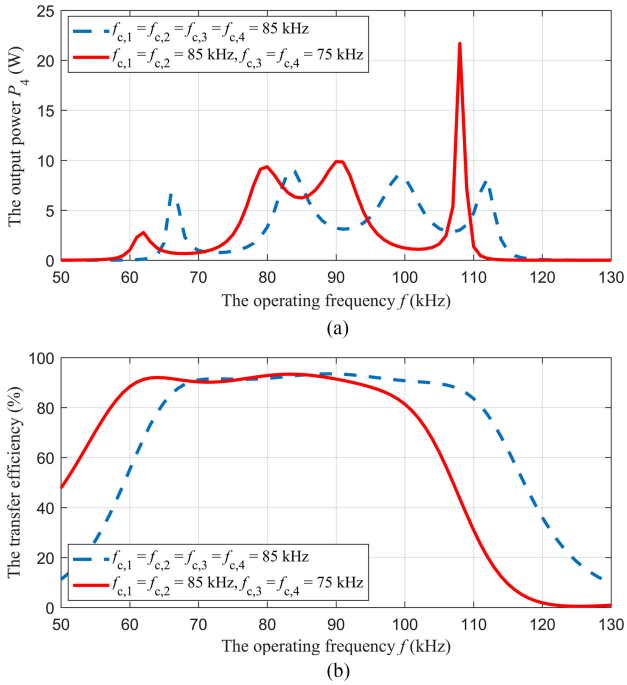

Fig. 2. Theoretical output power and transfer efficiency versus the operating frequency of a system with equal and unequal circuit's natural frequency.

According to the definition elucidated in Section III-A, we can get that resonance refers to the current amplitude on each circuit that is output power reaches a local maximum value. As shown in Fig. 2(a), there are four maximum power transfer points of each system, no matter the circuit's natural frequencies in the system are equal or not. The frequencies of the maximum power transfer points of each system are deviate from the circuit's natural frequencies in the system and are consistent well with the resonant frequencies calculated by (20), as listed in Table II. The results demonstrate that the resonant frequencies of an MC-WPT system have no direct relationship with circuit's natural frequencies in the system, which can be quickly and accurately determined by using (20).

TABLE III
MUTUAL INDUCTANCE COMBINATIONS OF THE EXAMPLES

Sequence number	Mutual inductances (μH)	Sequence number	Mutual inductances (μH)
The 1st example	$M_{12} = M_{23} = M_{34} = 31.69$; $M_{13} = M_{24} = 18.4$; $M_{14} = 10.93$	The 2nd example	$M_{12} = M_{23} = M_{34} = 18.4$; $M_{13} = M_{24} = 6.92$; $M_{14} = 3.12$
The 3rd example	$M_{12} = M_{23} = M_{34} = 10.98$; $M_{13} = M_{24} = 3.12$; $M_{14} = 1.28$	The 4th example	$M_{12} = M_{23} = M_{34} = 6.92$; $M_{13} = M_{24} = 1.66$; $M_{14} = 0.74$
The 5th example	$M_{12} = M_{23} = M_{34} = 4.55$; $M_{13} = M_{24} = 1.04$; $M_{14} = 0.508$	The 6th example	$M_{12} = M_{23} = M_{34} = 3.12$; $M_{13} = M_{24} = 0.744$; $M_{14} = 0.398$

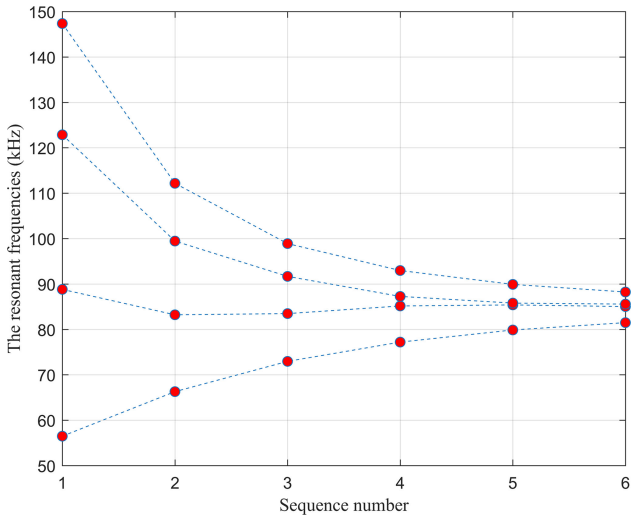

Fig. 3. Theoretical resonant frequencies under different mutual inductance combinations.

In addition, by comparing Fig. 2(a) and (b), we can get that the frequencies of the extreme points of output power and efficiency are not equal, but the power transfer at some resonant points are relatively efficient. Since all possible resonant points, including power and efficiency are determined, then the suitable resonant frequency can be selected as the operating frequency to balance power and efficiency.

B. Effects of Mutual Inductances

From (20), we can get that mutual inductance is a significant factor affecting resonant frequencies of MC-WPT systems. For illustration, the model used in Section IV-A is also used here. Excepting mutual inductance parameters, the other electric parameters are the same as listed in Table I. The four circuits' natural frequencies are set to $f_{c,1} = f_{c,2} = f_{c,3} = f_{c,4} = 85$ kHz by setting $C_1 = C_2 = C_3 = C_4 = 61.5$ nF.

For different mutual inductance combinations, as listed in Table III, the theoretical resonant frequencies calculated by (20) are plotted in Fig. 3 and the output power and efficiency versus the operating frequency of each example are plotted in Fig. 4 for comparison. To be more intuitively, only the output power

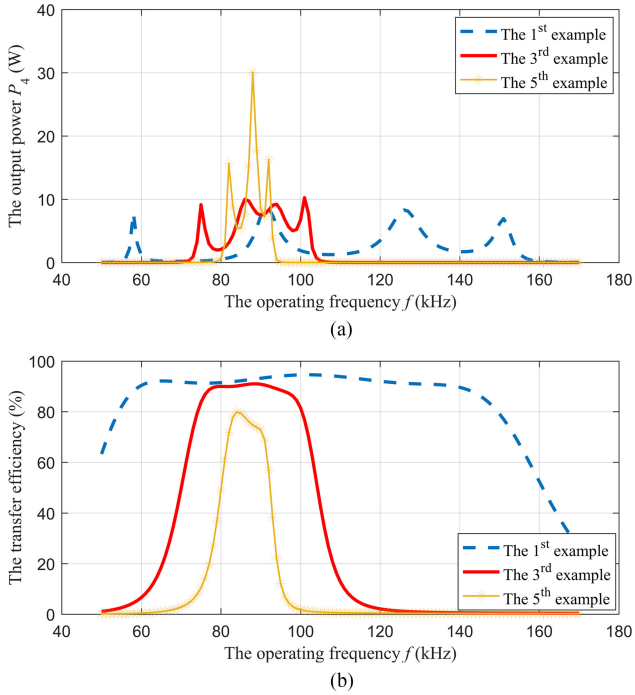

Fig. 4. Theoretical output power and transfer efficiency versus the operating frequency of the first, third, and fifth examples.

and efficiency curves of the examples of first, third, and fifth are plotted in Fig. 4.

As shown the examples of first, second, and third in Fig. 3, when the mutual inductances are very large, the four resonant frequencies are far apart. Corresponding to the examples of first and third in Fig. 4(a), there are four maximum power transfer points, whose frequencies are consistent well with the values listed in Fig. 3. With the decrease of mutual inductances, the four resonant frequencies are getting closer and some resonant frequencies may converge together, as the examples of fourth, fifth, and sixth shown in Fig. 3. Corresponding to the fifth example in Fig. 4(a), there are only three maximum power transfer points. The analysis results demonstrate that, no matter the system is in strong coupling or not, that is no matter there are resonant frequencies converge or not, output power reaches a local maximum when the operating frequency equals to one of the resonant frequencies calculated by (20), as shown in Fig. 3.

In addition, from Figs. 2(a) and 4(a), we can get that the circuit natural frequencies and mutual inductance have a great influence on the distribution of resonant points. Correspondingly, the power, especially the power of the resonant points will also be affected by CNF and mutual inductance. But whether the power is increased or decreased differs from resonant point to resonant point.

C. Effects of Load Resistance

Load resistance is another factor affecting the resonant frequencies of MC-WPT systems. Similarly, the model used in Section IV-A is used here for illustration. The four circuits' natural frequencies in the system are set to 85 kHz. For a load

TABLE IV
THEORETICAL SYSTEM'S NATURAL FREQUENCIES (SNF) AND RESONANT FREQUENCIES (RF)

SNF/kHz	66.13	82.83	99.85	112.63
RF/kHz (R_L = 1 Ω)	66.13	82.84	99.83	112.61
RF/kHz (R_L = 5 Ω)	66.29	83.21	99.45	112.14
RF/kHz (R_L = 50 Ω)	48.97	68.70	90.66	109.77

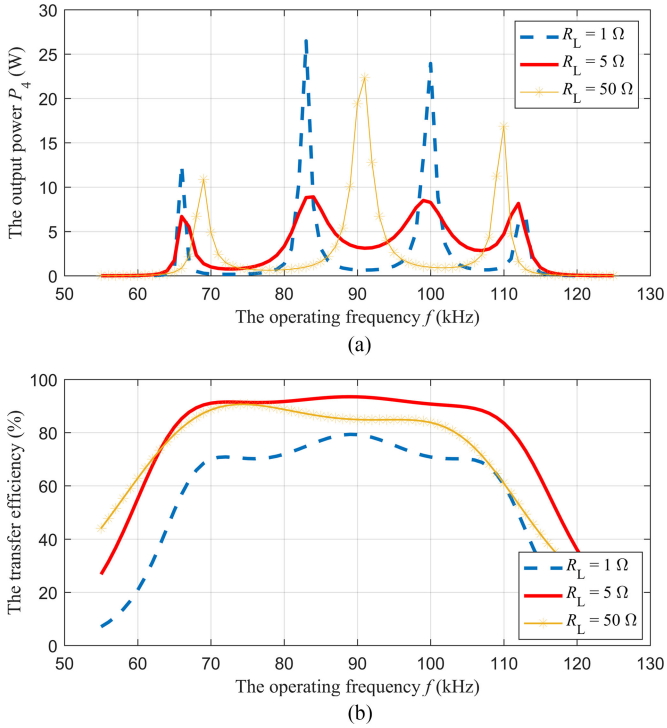

Fig. 5. For a load resistance of 1, 5, and 50 Ω, the output power and transfer efficiency versus the operating frequencies.

resistance of 1, 5, and 50 Ω, the theoretical system's natural frequencies calculated by (22) and resonant frequencies calculated by (20) are listed in Table IV. The theoretical output power and efficiency versus the operating frequency of the three examples are plotted in Fig. 5 for comparison.

As can be seen from Table IV, the resonant frequencies are very close to the system's natural frequencies when $R_{L4} \leq 5\ \Omega$, which demonstrate that the resonant frequencies equal to the SNF when the system is a weak damping system. However, when the system is a strong-damping system, as shown in Table IV, of the system with 50 Ω load resistance, the resonant frequencies are far deviate from the system's natural frequencies. Similarly, as shown in Fig. 5(a), the out power reaches a local maximum value when the operating frequency equals to the resonant frequencies rather than the system's natural frequencies. The results indicate that it is resonant frequencies rather than the SNF, which should be adopted as the actual operating frequency to realize system's resonant state. Only when the system is a weak damping system, are the n resonant frequencies of the system equal to the n system's natural frequencies.

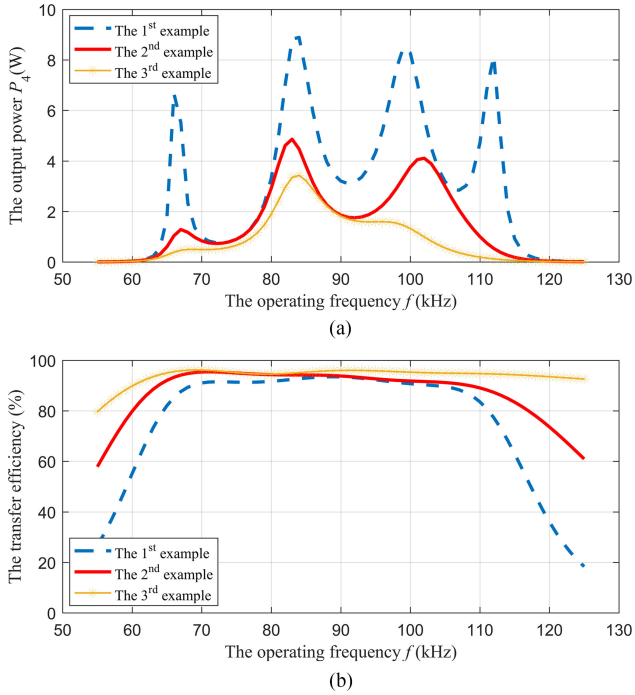

Fig. 6. Theoretical transfer power and efficiency versus the operating frequency with different system structures.

In addition, from Fig. 5(a), we can get that, when the system is a strong damping system ($R_L = 50\ \Omega$), the actual resonant points (the maximum power transfer points) may be less than the theoretical resonant points, as calculated in Table IV. That is because in some theoretical resonant points of a strong damping system, the energy could not oscillate and the system is equivalent to an overdamping system. But since all actual resonant points, including operating frequencies and corresponding output powers, are included in the theoretical results, then the actual resonant points can be quickly determined. Meanwhile, from Fig. 5(a), we can get that the change of resistance in small range has little effect on the distribution of resonant points, but it will affect the power level.

D. Effects of System's Structure

For a single-receiver MC-WPT system, if the quality factor of each oscillating circuit is large, the system can be regarded as weak-damping system [29]. However, for multi-receivers systems, even if the quality factor of each circuit is large, the system may not be regarded as a weak damping system. For illustration, three examples are conducted here for comparison. The first example is designed as a single-transmitter-two-repeaters-single-receiver system, the second example is set as a single-transmitter-single-repeater-two-receiver system, and the last example is a single-transmitter-three-receiver system. All circuits' natural frequencies of the three systems are set as 85 kHz and load resistances are set to 5 Ω. The other electric parameters are listed in Table I. The power received by R_{L4} (P_4) versus the operating frequencies of the three example are plotted in Fig. 6 for comparison. Since the resistances have no relationship with

TABLE V
THEORETICAL SYSTEM'S NATURAL FREQUENCIES (SNF) AND RESONANT FREQUENCIES (RF) OF THE THREE SYSTEMS

SNF/*kHz*	66.13	82.83	99.85	112.63
RF of the 1st example/*kHz*	66.29	83.21	99.45	112.12
RF of the 2nd example/*kHz*	66.44	82.51	101.72	109.98
RF of the 3rd example/*kHz*	66.20	83.14	99.26	111.6

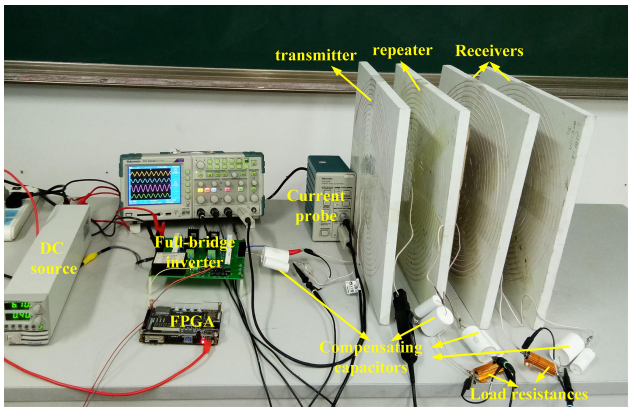

Fig. 7. Photograph of the experimental setup.

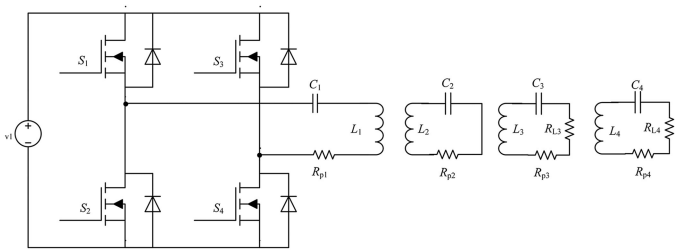

Fig. 8. Circuit schematic of the practical system.

system's natural frequencies, thus the system's natural frequencies of the three systems are equal. The system's natural frequencies calculated by (22) and resonant frequencies calculated by (20) of the three systems are listed in Table V.

V. SIMULATION AND EXPERIMENT VERIFICATION

A. Simulation and Experimental Setup

A practical single-transmitter-single-repeater-two-receiver system is built, as shown in Fig. 7, to verify the proposed theoretical model and analysis results. The circuit schematic of the system is shown in Fig. 8, where an H-bridge consisting of four MOSFETs is used as the voltage source and is coupled to the leftmost coil acting as the transmitter. The second coil is served as a repeater and the two rightmost coils are the receivers loading by a resistance, respectively. The four coils are set to be equal with the geometric parameters listed in Table VI and aligned to the coil centers $r = 0$ along the z-axis. In the experiments, the dc voltage is set as 7 V and the transfer distance between adjacent coils is fixed at 0.05 m. The electric parameters of the

TABLE VI
GEOMETRIC PARAMETERS OF THE PRACTICAL COILS

Parameters	Value
Number of turns	18
Inner radius of coil (m)	0.03
Width between per turn (m)	0.01
Radius of copper wire (m)	0.00125

TABLE VII
MEASURED ELECTRIC PARAMETERS OF THE SYSTEM

Parameters	Value
L_1, L_2, L_3, L_4 (μH)	57
R_{p1}, R_{p2}, R_{p3}, R_{p4} (Ω)	0.13
R_{L3}, R_{L4} (Ω)	5
M_{12}, M_{23}, M_{34} (μH)	6.92
M_{13}, M_{24} (μH)	3.11
M_{14} (μH)	7.9

TABLE VIII
THEORETICAL VALUE OF THE RESONANT POINTS

Resonant frequency(kHz)	Output power P_3 (W)	Output power P_4 (W)	Efficiency (%)
59	2.165	1.33	94.43
86	2.023	5.33	94.87
116	4.556	3.861	92.09
128	2.461	0.74	89.43

system are listed in Table VII, which are measured by using an *LCR* digital electric bridge (ZX8526A). The mutual inductance is obtained by means of two different measurements: the self-inductance L_1' of two series-connected coils and the self-inductance L_2' of the two coils connected in series-opposing. Hence, the mutual inductance between the two coils is calculated as $M = |L_1' - L_2'|/4$. The compensating capacitor of each coil is about 62 nF, then we can get that all the circuits' natural frequencies in the system are about 84.6 kHz. With the same electric parameters, the system can also be simulated in Simulink software for comparison.

B. Simulation and Experimental Results

For the given electric parameters, all possible resonant points of the system, including the resonant frequencies and corresponding output powers (P_3 and P_4) and efficiencies of resonant states are calculated, as shown in Table VIII. The theoretical, simulated, and measured output powers (P_3 and P_4) and transfer efficiencies versus the operating frequencies are plotted in Figs. 9 and 10, respectively.

As shown in Figs. 9 and 10, the theoretical output powers and efficiencies at arbitrary operating frequency are consistent well with the simulated results, which indicate that the proposed theoretical model in this paper is effective and accurate. There are some deviations between the theoretical and measured values, which is mainly caused by the measuring error of electrical parameters. In the experiments, the measuring error of self inductance and mutual inductance can be regarded as invariants, but the measuring error of resistance will increase with the increase of operating frequency due to resistance heating. According to

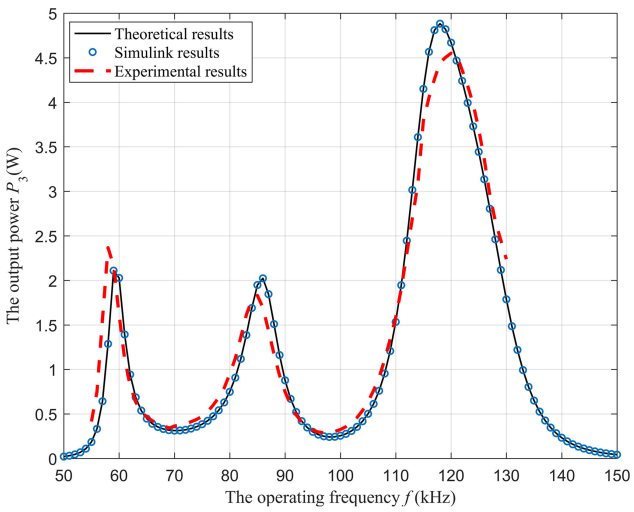

Fig. 9. Theoretical, simulated, and measured output power P_3 and P_4 versus the operating frequency. (a) Output power P_3 received by R_{L3}. (b) Output power P_4 received by R_{L4}.

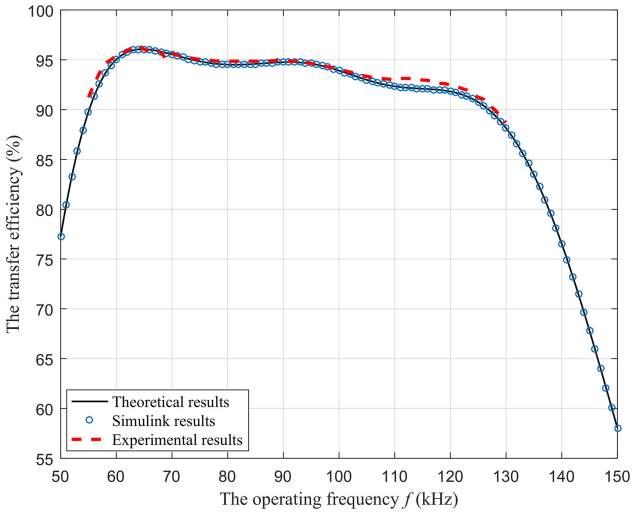

Fig. 10. Theoretical, simulated, and measured transfer efficiency versus the operating frequency.

the parameters analysis in Section IV, there is good reason to believe that the slight deviations of the distribution of resonant points and output power at 60 kHz and 86 kHz are due to the measuring error of self inductance and mutual inductance, and the derivation of power near 116 kHz is mainly caused by the error of resistance.

From Fig. 9, we can get that there are three actual resonant points of the system (59, 86, and 116 kHz), which are included in the theoretical results, as listed in Table VIII. The results indicate that all possible resonant points of the system, including resonant frequencies and corresponding output powers and efficiencies can be quickly and accurately determined by using (20), (15), and (16).

VI. Conclusion

A novel theoretical modeling and analysis method of integrating time domain and frequency domain is proposed in this paper, which suits for arbitrary MC-WPT systems without any parameter constraints to quickly and accurately determine their resonant points. Based on the proposed method, the generalized analytical expressions of resonant points of MC-WPT systems, including resonant frequencies and corresponding output powers and efficiencies at resonant states, are derived. Furthermore, the physical interpretation along with the mathematic relationship of several easy-confusing concepts, including CNF, SNF, and resonant frequency, are elucidated. It has been theoretically and experimentally demonstrated that it is resonant frequency rather than the CNF or SNF that should be adopted as the operating frequency to implement MC-WPT systems' resonant states. The analysis results provide a systematic theoretical criterion for the choice of operating frequency to achieve system's resonant state and to maintain reasonable energy efficiency against the variation of transfer distances and/or transfer orientation.

The derived analytical results would be potentially used to detect coupling factors and/or loads or other parameters for the MC-WPT systems because the resonant parameters are inherent to a system and are determined completely by its physical properties and their spatial distributions. In addition, the analytical current response on each circuit of a generalized WPT system with arbitrary number of transmitters, repeaters, and receivers is derived in this paper. Therefore, the proposed modeling and analysis method is particularly suitable for analyzing the characteristic of complicated multi-coil systems, such as multi-transmitters systems, multi-receivers systems, domino systems, etc., whose analytical performance functions are very difficult to obtain with the traditional analysis methods.

References

[1] A. Kurs, A. Karalis, R. Moffatt, J. D. Joannopoulos, P. Fisher, and M. Soljacic, "Wireless power transfer via strongly coupled magnetic resonances," *Science*, vol. 317, pp. 83–86, Jul. 2007.

[2] A. Karalis, J. D. Joannopoulos, and M. Soljačić, "Efficient wireless non-radiative mid-range energy transfer," *Ann. Phys.*, vol. 323, pp. 34–48, Apr. 2008.

[3] J. Chen, S. Li, S. Chen, S. He, and Z. Shi, "Q-charge: A quadcopter-based wireless charging platform for large-scale sensing applications," *IEEE Netw.*, vol. 31, no. 6, pp. 56–61, Nov./Dec. 2017.

[4] D. Kurschner, C. Rathge, and U. Jumar, "Design methodology for high efficient inductive power transfer systems with high coil positioning flexibility," *IEEE Trans. Ind. Electron.*, vol. 60, no. 1, pp. 372–381, Jan. 2013.
[5] A. K. RamRakhyani and G. Lazzi, "Multicoil telemetry system for compensation of coil misalignment effects in implantable systems," *IEEE Antennas Wireless Propag. Lett.*, vol. 11, pp. 1675–1678, Dec. 2012.
[6] B. H. Waters, A. P. Sample, P. Bonde, and J. R. Smith, "Powering a ventricular assist device (VAD) with the free-range resonant electrical energy delivery (FREE-D) system," *Proc. IEEE*, vol. 100, no. 1, pp. 138–149, Jan. 2012.
[7] J. Huh, S. W. Lee, W. Y. Lee, G. H. Cho, and C. T. Rim, "Narrow-width inductive power transfer system for online electrical vehicles," *IEEE Trans. Power Electron.*, vol. 26, no. 12, pp. 3666–3679, Dec. 2011.
[8] C. Hu, Y. Sun, X. Lv, Z. Wang, and Q. Xiong, "Magnetic coupler design procedure for IPT system and its application to EVs' wireless charging," *Int. J. Appl. Electromagn. Mech.*, vol. 47, pp. 861–873, May. 2015.
[9] S. Y. R. Hui, W. Zhong, and C. K. Lee, "A critical review of recent progress in mid-range wireless power transfer," *IEEE Trans. Power Electron.*, vol. 29, no. 9, pp. 4500–4511, Sep. 2014.
[10] W. X. Zhong, C. Zhang, X. Liu, and S. Y. R. Hui, "A methodology for making a three-coil wireless power transfer system more energy efficient than a two-coil counterpart for extended transfer distance," *IEEE Trans. Power Electron.*, vol. 30, no. 2, pp. 933–942, Feb. 2015.
[11] W. Zhang, S. Wong, C. K. Tse, and Q. Chen, "Design for efficiency optimization and voltage controllability of series–series compensated inductive power transfer systems," *IEEE Trans. Power Electron.*, vol. 29, no. 1, pp. 191–200, Jan. 2014.
[12] Z. Ye, Y. Sun, X. Dai, C. Tang, Z. Wang, and Y. Su, "Energy efficiency analysis of u-coil wireless power transfer system," *IEEE Trans. Power Electron.*, vol. 31, no. 7, pp. 4809–4817, Jul. 2016.
[13] A. P. Sample, D. A. Meyer, and J. R. Smith, "Analysis, experimental results, and range adaptation of magnetically coupled resonators for wireless power transfer," *IEEE Trans. Ind. Electron.*, vol. 58, no. 2, pp. 544–554, Feb. 2011.
[14] Y. Zhang, Z. Zhao, and K. Chen, "Frequency-splitting analysis of four-coil resonant wireless power transfer," *IEEE Trans. Ind. Appl.*, vol. 50, no. 4, pp. 2436–2445, Jul. 2014.
[15] J. Park, Y. Tak, Y. Kim, Y. Kim, and S. Nam, "Investigation of adaptive matching methods for near-field wireless power transfer," *IEEE Trans. Antennas Propag.*, vol. 59, no. 5, pp. 1769–1773, Nov. 2011.
[16] T. C. Beh, M. Kato, T. Imura, S. Oh, and Y. Hori, "Automated impedance matching system for robust wireless power transfer via magnetic resonance coupling," *IEEE Trans. Ind. Electron.*, vol. 60, no. 9, pp. 3689–3698, Sep. 2013.
[17] N. Y. Kim, K. Y. Kim, and C. W. Kim, "Automated frequency tracking system for efficient mid-range magnetic resonance wireless power transfer," *Microw. Opt. Technol. Lett.*, vol. 54, pp. 1423–1426, Aug. 2012.
[18] Y. Lim, H. Tang, S. Lim, and J. Park, "An adaptive impedance-matching network based on a novel capacitor matrix for wireless power transfer," *IEEE Trans. Power Electron.*, vol. 29, no. 8, pp. 4403–4413, Aug. 2014.
[19] H. Li, K. Wang, L. Huang, W. Chen, and X. Yang, "Dynamic modeling based on coupled modes for wireless power transfer systems," *IEEE Trans. Power Electron.*, vol. 30, no. 11, pp. 6245–6253, Nov. 2015.
[20] H. Nguyen and J. I. Agbinya, "Splitting frequency diversity in wireless power transmission," *IEEE Trans. Power Electron.*, vol. 30, no. 11, pp. 6088–6096, Nov. 2015.
[21] W. Niu, W. Gu, J. Chu, and A. Shen, "Frequency splitting patterns in wireless power relay transfer," *IET Circuits Devices Syst.*, vol. 8, pp. 561–567, Jul. 2014.
[22] S. Cheon, Y. H. Kim, S. Y. Kang, M. L. Lee, and J. M. Lee, "Circuit-model-based analysis of a wireless energy-transfer system via coupled magnetic resonances," *IEEE Trans. Ind. Electron.*, vol. 58, no. 7, pp. 2906–2913, Jul. 2011.
[23] W. Niu, J. Chu, W. Gu, and A. Shen, "Exact analysis of frequency splitting phenomena of contactless power transfer systems," *IEEE Trans. Circuits Syst. I, Reg. Papers*, vol. 60, no. 6, pp. 1670–1677, Jun. 2013.
[24] W. Q. Niu, W. Gu, J. X. Chu, and A. D. Shen, "Coupled-mode analysis of frequency splitting phenomena in CPT systems," *Electron. Lett.*, vol. 48, pp. 723–724, Jun. 2012.
[25] B. H. Waters, B. J. Mahoney, V. Ranganathan, and J. R. Smith, "Power delivery and leakage field control using an adaptive phased array wireless power system," *IEEE Trans. Power Electron.*, vol. 30, no. 11, pp. 6298–6309, Nov. 2015.
[26] M. Fu, T. Zhang, X. Zhu, P. C. Luk, and C. Ma, "Compensation of cross coupling in multiple-receiver wireless power transfer systems," *IEEE Trans. Ind. Inform.*, vol. 12, no. 2, pp. 474–482, Apr. 2016.
[27] W. Zhong and S. Y. R. Hui, "Auxiliary circuits for power flow control in multifrequency wireless power transfer systems with multiple receivers," *IEEE Trans. Power Electron.*, vol. 30, no. 10, pp. 5902–5910, Oct. 2015.
[28] D. Ahn and S. Hong, "Effect of coupling between multiple transmitters or multiple receivers on wireless power transfer," *IEEE Trans. Ind. Electron.*, vol. 60, no. 7, pp. 2602–2613, Jul. 2013.
[29] Y. Sun, Z. Liao, Z. Ye, C. Tang, and P. Wang, "Determining the maximum power transfer points for MC-WPT systems with arbitrary number of coils," *IEEE Trans. Power Electron.*, vol. 33, no. 11, pp. 9734—9743, Nov. 2018.
[30] W. Fu, B. Zhang, D. Qiu, and W. Wang, "Maximum efficiency analysis and design of self-resonance coupling coils for wireless power transmission system," *Proc. CSEE*, Jun. 2009, pp. 21–26.
[31] J. H. Fu and Z.-Fang, *Modal Analysis*. Oxford, U.K.: Butterworth Heinemann, 2001.

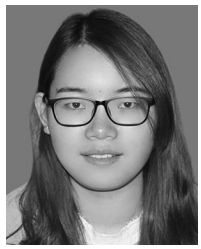

Zhi-Juan Liao received the B.E. degree, in 2014, from the College of Automation, Chongqing University, Chongqing, China, where she is currently working toward the Ph.D. degree in control theory and control engineering.

Her research interests include wireless power transfer and power electronics.

Yue Sun (M'07) received the B.E. degree in electrical engineering, the M.E. degree in industry automation, and the Ph.D. degree in mechanical electrical integrated manufacturing from Chongqing University, Chongqing, China, in 1982, 1988, and 1995, respectively.

In 1997, he was a Senior Visiting Scholar in France for one year. He is currently a Professor with the State Key Laboratory of Power Transmission Equipment and System Security and New Technology, and the College of Automation, Chongqing University. His research interests include automatic control, wireless power transfer, and power electronics applications.

Zhao-Hong Ye received the B.E. and M.E. degrees, in 2008 and 2011, respectively, from the College of Automation, Chongqing University, Chongqing, China, where he is currently working toward the Ph.D. degree in control theory and control engineering.

He is currently working as a Lecturer with the College of Automation, Chongqing University. His research interests include wireless power transfer, power electronics applications, and intelligent control.

Chun-Sen Tang (S'08–M'09) received the B.E. and Ph.D. degrees from the College of Automation, Chongqing University, Chongqing, China, 2004 and 2009, respectively.

In 2008, he was a Research Fellow with the Department of Electrical and Computer Engineering, The University of Auckland, Auckland, New Zealand. He joined the College of Automation, Chongqing University, Chongqing, in 2009 and he is currently an Associate Professor. His current research interests include non-linear modeling and analysis, intelligent control, and wireless power transfer.

Pei-Yue Wang received the B.E. degree from the College of Mechanical and Electrical Engineering, Xidian University, Xi'an, China, in 2015. He is currently working toward the Ph.D. degree in control theory and control engineering at the College of Automation, Chongqing University, Chongqing, China.

His research interests include modeling and control of wireless power transfer and power electronics.